iScience

CellPress

Article

A Heavily Surface-Doped Polymer with the Bifunctional Catalytic Mechanism in Li-O_2 Batteries

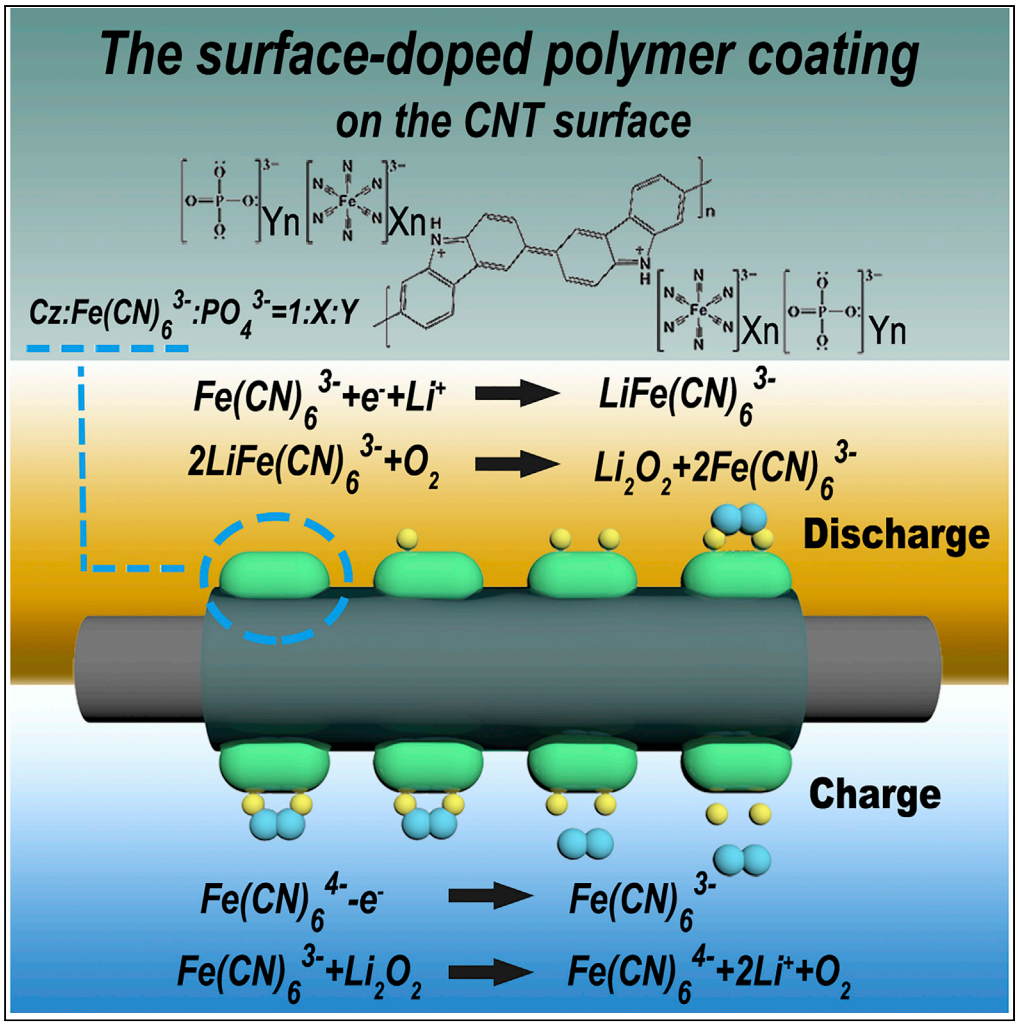

Chengyang Xu, Langyuan Wu, Shifan Hu, Huamei Xie, Xiaogang Zhang

azhangxg@nuaa.edu.cn

HIGHLIGHTS

A controllable electrochemical method to introduce redox-active anions in CP matrixes

Doping levels and semiconductor properties of CPs can be effectively controlled

Surface-doped CPs have better redox properties and electrochemical stability

The PCz doped by functionalized dopants shows a good catalytic effect

Xu et al., iScience *14*, 312–322
April 26, 2019
https://doi.org/10.1016/j.isci.2019.03.016

iScience

CellPress

Article

A Heavily Surface-Doped Polymer with the Bifunctional Catalytic Mechanism in Li-O_2 Batteries

Chengyang Xu,[1] Langyuan Wu,[1] Shifan Hu,[1] Huamei Xie,[1] and Xiaogang Zhang[1,2,*]

SUMMARY

The application of conducting polymers (CPs) in energy storage systems is greatly limited by insufficient reversibility and stability. Here, we successfully incorporated functionalized dopants ($Fe(CN)_6^{3-}$ [FCN] and PO_4^{3-} ions) in CPs matrixes to achieve a preferable electrochemical performance. A stable cation inserting/expulsing behavior of surface-doped polycarbazole (PCz) is demonstrated in our work, where doping levels and semiconductor properties of PCz are effectively controlled to adjust their redox properties and stability. With carbon nanotube (CNT) films as the substrate, the CNT/PCz:FCN composite is initially adopted as a free-standing catalytic electrode in Li-O_2 cells. The molecule-level dispersed FCN dopants on the surface can work as bifunctional redox mediators on the charge-discharge process. Thus, this composite can not only achieve a low charge plateau of 3.62 V and a regular growth of capacities from 1,800 to 4,800 mAh/g_{CNT}, but also maintain the most of charge voltages under 4.0 V for 150 cycles.

INTRODUCTION

One ground-breaking polymer class with high relevance to the electronics and energy systems are conducting polymers (CPs), where conductivity is often enabled by the macromolecules possessing π-conjugation in polymer backbones (Ehsani et al., 2018; Kim et al., 2017; Zhan et al., 2018; Zhou and Shi, 2016). CPs have been crucial for a host of new applications owing to the adjustable conductivity and optical properties. However, their applications in energy storage devices (Shi et al., 2015) are not as good as that in organic light-emitting diodes (Burn et al., 1997) or photovoltaic devices (Xia et al., 2008). Although p-type CPs have been researched as electrode materials for Li-ion batteries and supercapacitors, their performance was influenced by the insufficient reversibility and limited degree of doping as well as the electrochemical stability caused by the overoxidation (MacDiarmid, 2001). Meanwhile, n-type π-conjugated polymers also suffer from inevitable challenges such as low redox potentials and environmental instability (Klavetter and Grubbs, 1988; Song et al., 2014).

Recently, a particularly promising strategy is the introduction of functionalized anions into CP matrixes so as to enhance the electronic conductivity and tailor their redox potentials and specific capacities, where the redox mechanism of CPs is transformed from p-type doping of large anions to n-type doping of small cations (Pron and Rannou, 2002; Qi and Pickup, 1998; Rajesh et al., 2004; Zhou et al., 2011). Thus, the above-mentioned barriers could be effectively overcome since CPs doped by functionalized anions could simultaneously achieve better electrochemical utilization and cycling stability. The incorporation of functionalized dopants is an alternative and simpler strategy for the improvements of basic characteristics of CPs since most of monomers can be directly used without the complicated synthetic procedures. There are several advantages of these doped CPs (Pron and Rannou, 2002), including (1) providing abundant redox sites for the energy storage, (2) working as reaction mediators to facilitate the electron transfer, and (3) more chemically and electrochemically stable than intrinsic n-type and p-type polymers. Therefore, this promising strategy is expected to provide a mass of materials useful for electrocatalysis and energy storage devices (Song and Palmore, 2006).

These surface-doped conjugated polymers are especially suitable as a free-standing catalytic electrode for the application in Li-O_2 cells, which urgently need to face several major challenges such as high overpotentials, limited cycling life, and low rate capability (Aurbach et al., 2016; Christensen et al., 2012; Lu et al., 2014). These challenges are mainly caused by the insulating nature of discharge products Li_2O_2 in nonaqueous solutions. The extra energy for the decomposition of Li_2O_2 can simultaneously lead to Li_2CO_3

[1]College of Material Science and Technology & Jiangsu Key Laboratory of Electrochemical Energy Storage Technologies, Nanjing University of Aeronautics and Astronautics, Nanjing 210016, P.R. China

[2]Lead Contact

*Correspondence: azhangxg@nuaa.edu.cn

https://doi.org/10.1016/j.isci.2019.03.016

formation and electrolyte decomposition, accompanying with side products accumulating on the electrode surface (McCloskey et al., 2012a, 2012b; Ottakam et al., 2013). In fact, inorganic catalysts have been widely adopted to combine with carbon matrices to facilitate the decomposition of products (McCloskey et al., 2012a; Xu et al., 2013). However, parasitic reactions at the Li_2O_2/carbon interphase as well as the decomposition of electrolyte are inevitable owing to their unselective catalytic activity (Kim and Park, 2017). As for this new type of CPs-supported heterogeneous catalyst, their surface conductivity and catalytic activity can be easily controlled by the types and doping levels of redox-active dopants (Milczarek and Inganas, 2012; Pron and Rannou, 2002; Song and Palmore, 2006). Moreover, since these dopants containing catalytically active centers are molecularly dispersed on the CPs surface, they can provide a lot of homogeneous redox sites for the formation and decomposition of Li_2O_2. Meanwhile, the protective layers of CPs have been reported to effectively suppress side reactions at the carbon electrode/organic electrolyte interface and improve the cycling performance of Li-O_2 cells (Amanchukwu et al., 2016; Kim and Park, 2017).

Hence, we proposed a controllable electrochemical method to introduce functionalized anions in CP matrixes for an adjustable electrochemical performance. The polycarbazyl (PCz) is electro-doped by $Fe(CN)_6^{3-}$ (FCN) and PO_4^{3-} (PO) ions with different ratios. The FCN ions are adopted to improve the conductivity of PCz and provide abundant redox-active sites for electrochemical processes. As for the assistant dopants of PO, they can effectively prevent the saturation of FCN content in the PCz matrixes and the attenuation of electrochemical responses. The synergistic effect of two dopants convert the ion exchange mechanism of PCz from a p-type behavior into a stable cation inserting/expulsing behavior. With carbon nanotube (CNT) films as the substrate, the obtained composite of CNT/PCz:FCN is directly adopted as a free-standing electrode in Li-O_2 cells. The electrochemical results of a low charge plateau, a regular growth of capacities and an enhanced cycling performance, are achieved by the bifunctional catalysis and high stability of PCz:FCN coatings.

RESULTS

In fact, the ion transport processes of polypyrrole (PPy) bulk doped with FCN ions during the polymerization has been researched in earlier reports (Qi and Pickup, 1998; Rajesh et al., 2004; Zhou et al., 2011). Those results demonstrated that, when FCN ions were immobilized in PPy matrixes by the electrostatic interaction, the redox switching of doped polymers could be easily realized by the d–π electronic transitions. Simultaneously, an n-type doping behavior has been discovered that the cations were inserted to compensate the negative charge generated by FCN ions.

In this work, a controllable electrochemical method is proposed for the doping of FCN ions on the surface of PCz after the polymerization. This method is beneficial to control the doping levels and semiconductor properties of the composite, which are important evidences to explain how to achieve a preferable electrochemical performance. In addition, the stabilizing effect of PO dopants is definitely emphasized for the stability of electrochemical responses that is still identified as a problem for bulk-doped CPs (Kim and Song, 2015).

The Mechanism of Transformation of Ion Transport Processes of Surface-Doped PCZ

The electrochemical polymerization of PCz films is demonstrated by cyclic voltammetry (CV), and the ongoing doping/dedoping processes are *in situ* monitored by the electrochemical quartz crystal microbalance (EQCM) method. The PCz films were prepared by 10 successive voltammetry cycles with a scan rate of 0.1 V s^{-1} so as to obtain a thin and uniform polymer film. As the first scan shown in Figure 1A, the only anodic peak around 0.9 V corresponds with the formation of cation radicals, which tends to form the main product 3,3′-bicarbazyl (Karon and Lapkowski, 2015). Since 3-3′-dicarbazyl is more readily oxidized than carbazole, the increasing peak currents around 0.6 V demonstrate that the degree of polymerization increases with repetitive scans. It is worth mentioning that irreversible peaks at −0.05 V may be caused by oxygen species of the Au electrode, simultaneously appearing in CV curves of as-synthesized PCz.

The second doping process of as-synthesized PCz is realized by the potentiostatic methods in aqueous solutions with FCN as redox-active dopants and PO as assistant dopants (see Figure S1). The electrochemical performance of surface-doped PCz was monitored in nonaqueous solutions, and thus the release of dopants could be effectively suppressed because of their poor dissolubility. Different redox properties in Figure 1B imply that ClO_4^- anions doping process of undoped PCz around a higher potential of 0.6 V may be fully restricted for the surface-doped PCz. Moreover, the EQCM results also reveal the opposite

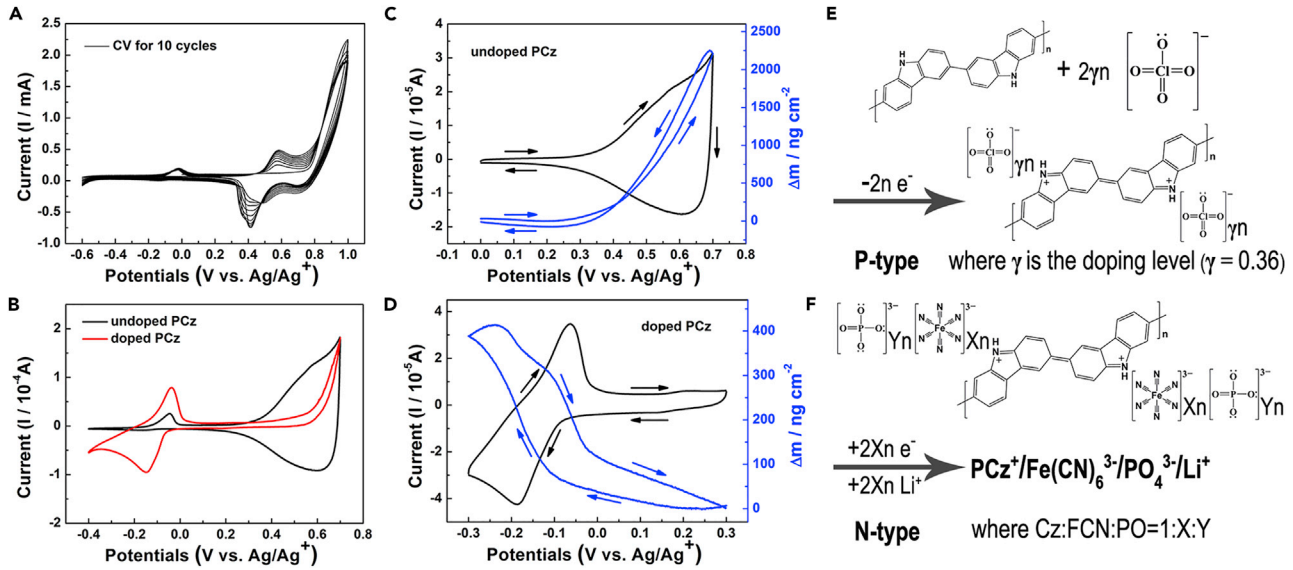

Figure 1. Polymerization and Redox Properties of Doped/Undoped PCz

Voltammograms in a 0.1 M $LiClO_4$/acetonitrile solution of (A) the polymerization of carbazole monomers from −0.6 to 1.0 V vs. Ag/Ag^+ at a scan rate of 100 mV s^{-1} and (B) the redox properties of doped/undoped PCz from −0.4 to 0.7 V vs. Ag/Ag^+ at 50 mV s^{-1}. Gravimetric responses and corresponding voltammograms in different voltage range as well as schematic diagrams of the charge compensation of (C and E) undoped PCz and (D and F) surface-doped PCz.

trend of mass changes for two electrodes (Figure S2A). Owing to intrinsic properties of the p-type semiconductor, the mass of PCz could increase with the inserting of anions when it is oxidized. On the contrary for surface-doped PCz, an apparent reduction peak and an increase of mass at negative potentials suggest that it shows a stable n-type behavior.

The EQCM methods are always adopted to explore charge compensation mechanisms of CPs through linking mass changes to contributing counter ions as well as solvent molecules (Hillman, 2011). The mass change per unit area (Δm/ng cm^{-2}) is determined via the resonant frequency change (Δf/Hz) on the basis of the well-known Sauerbrey equation (see Transparent Methods), where a proportionality factor of 6.838 ng cm^{-2} Hz^{-1} was obtained for the numeric conversion of 8 MHz AT-cut quartz crystals. To further study ion transport processes, EQCM responses were recorded in a limited voltage range corresponding to the reversible redox peaks in Figure 1B. The voltammetry curves and the corresponding Δm versus V plots are presented in Figures 1C and 1D. The observed behavior in Figure 1C is typical for p-type PCz films, where the mass of the electrode is increased with enhanced anodic potentials by the incorporation of ClO_4^- anions. The equivalent molar mass (M) was obtained by the slope of Δm-Q plots based on the Faraday's law (Figures S2B and 2C). This value of M is 35.82 g mol^{-1} for anions when losing one electron and deviates from the molar mass of ClO_4^- anion (99.5 g mol^{-1}), implying a limited doping level of 0.36 in the p-type PCz as illustrated in Figure 1E. As reported, this phenomenon may be caused by the compensation of co-ion transfer in the opposite direction or the mass loss of p-type polymers due to the overoxidation (Baba et al., 2004; Tóth et al., 2015). As for the surface-doped PCz films, the increase and decrease of mass are discovered, respectively, in cathodic and anodic scans, which demonstrate an n-type doping behavior with the exchange of cations. The doping level of cations depends on the content of FCN dopants on the basis of the charge compensation mechanisms (Figure 1F). It is difficult to confirm the molar mass of cations for the interruptions of solvent molecules, whereas the carbazole/FCN ratios will be discussed in later sections.

The Synergistic Effect of Two Dopants on the Adjustable Electrochemical and Semiconducting Performance

We investigate the effect of two dopants of FCN and PO as well as their concentrations in solutions and present a quantitative study of semiconducting properties (including flat band potentials, carrier concentrations, and band gaps) using electrochemical techniques and spectroscopy. The voltammetry curves of PCz doped respectively and simultaneously by FCN and PO ions with the substrate of a glassy carbon electrode are shown in Figure 2A. Although the dopant of FCN is crucial to the electro-activity, it can cause a

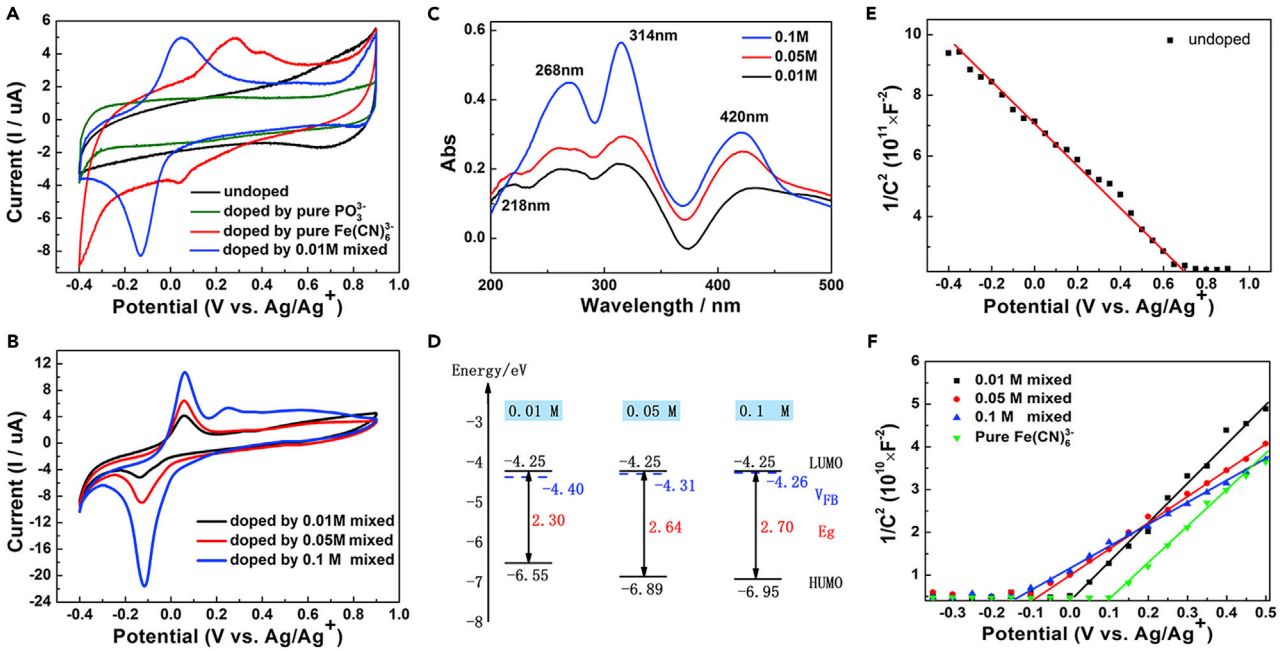

Figure 2. The Electrochemical and Spectral Responses of PCz Doped by Two Dopants with Different Ratios

(A and B) Voltammograms of PCz films undoped and doped by (A) pure and mixed solutions as well as (B) mixed solutions with different concentrations on the substrate of a glassy carbon from -0.4 V to 0.9 V vs Ag/Ag^+ at 20 mV s^{-1}.

(C) UV-vis absorption spectra and (D) corresponding energy level diagram of PCz films doped by different mixed solutions on the ITO substrate.

(E and F) Mott–Schottky plots of PCz films (E) undoped and (F) doped by pure and mixed solutions on the substrate of a glassy carbon.

peak separation and a higher asymmetric redox peak as illustrated when used as the only dopant. Similar results have also been reported that polymer films could be saturated with FCN ions, leading to the attenuation of electrochemical responses (Qi and Pickup, 1998). The synergistic effect of two dopants is attributed to the stabilization of PO on the doping processes since we found mixed solutions did not experience a degradation process with obvious color changes that appeared in pure solutions of FCN (Figure S3). The influence of the concentrations of FCN in mixed solutions is illustrated in Figure 2B. The concentration of PO ions in mixed solutions is always 0.1 M and the concentrations of mixed solutions correspond to that of FCN ions. As illustrated, the peak currents increase regularly with increasing concentrations of FCN, which implies that a higher doping level may be achieved by more dopants in doping solutions.

The UV-visible spectrum of electro-deposited films on the indium tin oxide (ITO) substrate (Figure 2C) is attributed to the π-conjugation of PCz and colorful dopant of FCN. The tiny blue shifts of the maximum of absorption at nearly 314 and 420 nm and the lost peaks of 0.1 M mixed solutions at 218 and 268 nm may imply the enhancement of dopant-to-ligand (d-π) charge transfer transitions and the weakening of π-π* electron transition (Yu et al., 2014). Moreover, the obviously increased absorption intensities mean that increased concentrations definitively lead to a higher doping level. The optical band gap (Eg) of surface-doped PCz was obtained from $(\alpha h\nu)^2 \sim h\nu$ curves, and the values of Eg were estimated from the extrapolation of the linear region (Mozaffari et al., 2012) (Figure S4). The band gaps of PCz films doped by different solutions range from 2.3 to 2.7 eV. The lowest unoccupied molecular orbital energy levels, obtained from reduction onset, keep at around 4.25 eV from vacuum. Thus, the highest occupied molecular orbital energy levels can be calculated from the above data and vary from 6.55 to 6.95 eV (Figure 2D), which is expected to make n-type CPs stable during the charging of Li-O_2 cells under oxygen environments owing to the ability of standing a pretty high overpotentials (Boudreault et al., 2007).

Mott-Schottky (M-S) measurements were implemented to study the semiconducting nature such as flat band potentials (V_{FB}) and densities of charge carriers. M-S plots are always adopted to describe variations of space-charge capacitance, which is constructed by the M-S equation (Hamadou et al., 2013):

$$\frac{1}{C_{SC}{}^2} = \frac{2}{\varepsilon\varepsilon_0 eN}\left(V - V_{FB} - \frac{kT}{e}\right) \qquad \text{(Equation 1)}$$

where C_{sc} is the capacitance of the space charge region, ε is the dielectric constant of the polymer, ε_0 is the permittivity of free space, N is the carrier density (electron donor concentration for an n-type semiconductor or hole acceptor concentration for a p-type semiconductor), V is the applied potentials, and V_{FB} is the flat band potential. The positive and negative slopes of M-S plots indicate, respectively, n-type and p-type conductance, and the size of these slopes determine densities of charge carriers in the semiconductor. If we take α as the slope of the straight line of $1/C_{sc}^2$ versus V plots, then the carrier density can be obtained with the following equation:

$$N = \left(\frac{2}{\varepsilon\varepsilon_0 e\alpha}\right) \quad \text{(Equation 2)}$$

Therefore, as illustrated in Figures 2E and 2F, the undoped and surface-doped PCz exhibit, respectively, a p-type and n-type behavior. Simultaneously, the carrier density is inversely proportional to the slope of the straight line and the variation of relative slopes indicates that the densities of donor carriers of doped PCz are higher than that of accepter carriers of undoped PCz. Moreover, higher doping levels can further improve the densities of charge carriers (Figure 2F), which has also been reported that conductivity of CPs can be varied over orders of magnitude (Liang et al., 2015). The V_{FB} of PCz is determined by the intercept of linear regions of plots on the horizontal axis and the values range from 0.1 to −0.14 V for different doping solutions. The V_{FB} is necessary to reduce the band bending to zero, and the distance between V_{FB} and orbital energy levels can create a relaxation effect. The decrease of V_{FB} for n-type semiconductor can shorten the above-mentioned distance of energy levels and facilitate the transfer of charge carriers (Figure 2D). Hence, the excellent electrochemical performance of PCz doped by two dopants is attributed to better n-type semiconducting properties, including more charge carriers, lower flat band potentials, and higher band gaps.

The Surface Composition and Doping Levels of CNT/PCz:FCN Composites

The CNT/PCz:FCN composite was prepared directly as the air electrode since CNT films can provide large surface area for the deposition of PCz and improve the conductivity of the whole electrode for better rate capability. The polymerization and doping processes of the as-synthesized composite are the same as that on substrates of glassy carbon and ITO. To examine the surface morphologies of composites, transmission electron microscopy (TEM) was carried out. As the TEM images show in Figures 3A and 3B, the surface of CNT fibers appear to be amorphous without obvious lattice fringes and covered by an organic coating layer, which is expected of PCz:FCN composites. For the determination of the thickness of coating layers, we chose a small region where the CNT fiber was not fully covered by the polymer. As is pointed with the red lines in Figure 3B, several lattice fringes imply the border of nanotubes with smooth side walls, and the thickness of surface-doped polymers based on the homogeneous part of coating layers is estimated to be 4 nm. The element distribution on the surface was investigated by energy-dispersive X-ray spectroscopy (EDS). There are obvious distributions of Fe and N elements along nanotube fibers according to the EDS observation (Figure S5). In addition, the new peaks at 2,054 and 1,022 cm^{-1} in Fourier transform infrared spectra (Figure S6) are, respectively, responding to the –CN group of $Fe(CN)_6^{3-}$ and the –PO group of PO_4^{3-} (Arrondo et al., 1984; Pandey and Panday, 2016). Thus, we confirmed qualitatively the composition of CNT/PCz:FCN composites as in the schematic diagram in Figure 3C, although polymer layers are not ideally uniform because of the main existence of PCz as oligomers.

For the quantitative study of doping levels in the PCz, X-ray photoelectron spectroscopy (XPS) was performed at the CNT/PCz composites, which are undoped and doped by 0.01, 0.05, 0.1 M mixed solutions and a 0.1 M pure FCN solution. As illustrated in Figure 3D, element contents of Fe and N of samples increase regularly from the bottom up in the following order: undoped, doped by 0.01 and 0.05 M mixed solutions, doped by pure FCN solutions, and 0.1 M mixed solutions. Since the C-N bonds appear simultaneously in PCz and FCN, the N 1s spectrum was analyzed as the main evidence to estimate molar ratios of the unit of PCz and dopants. For the undoped sample (Figure 3E), the peak at 400 eV corresponds to the organic C-N bond in the penta heterocycles of carbazole molecules, and two peaks over 401 eV indicate the higher valence of carbazole. The new peak at 398 eV for doped samples represents the inorganic C-N bond of $Fe(CN)_6^{4-}$/$Fe(CN)_6^{3-}$ ions. With the increase of doping contents in Figures 3F–3I, the stronger new peak for dopants at 398 eV, the weaker peak for carbazole molecules over 400 eV. The molar ratios of Cz:FCN were estimated from the relative area of peaks for different C-N bonds and the growth trend of molar ratios is the same as that of Fe contents in the polymer (Figure S7).

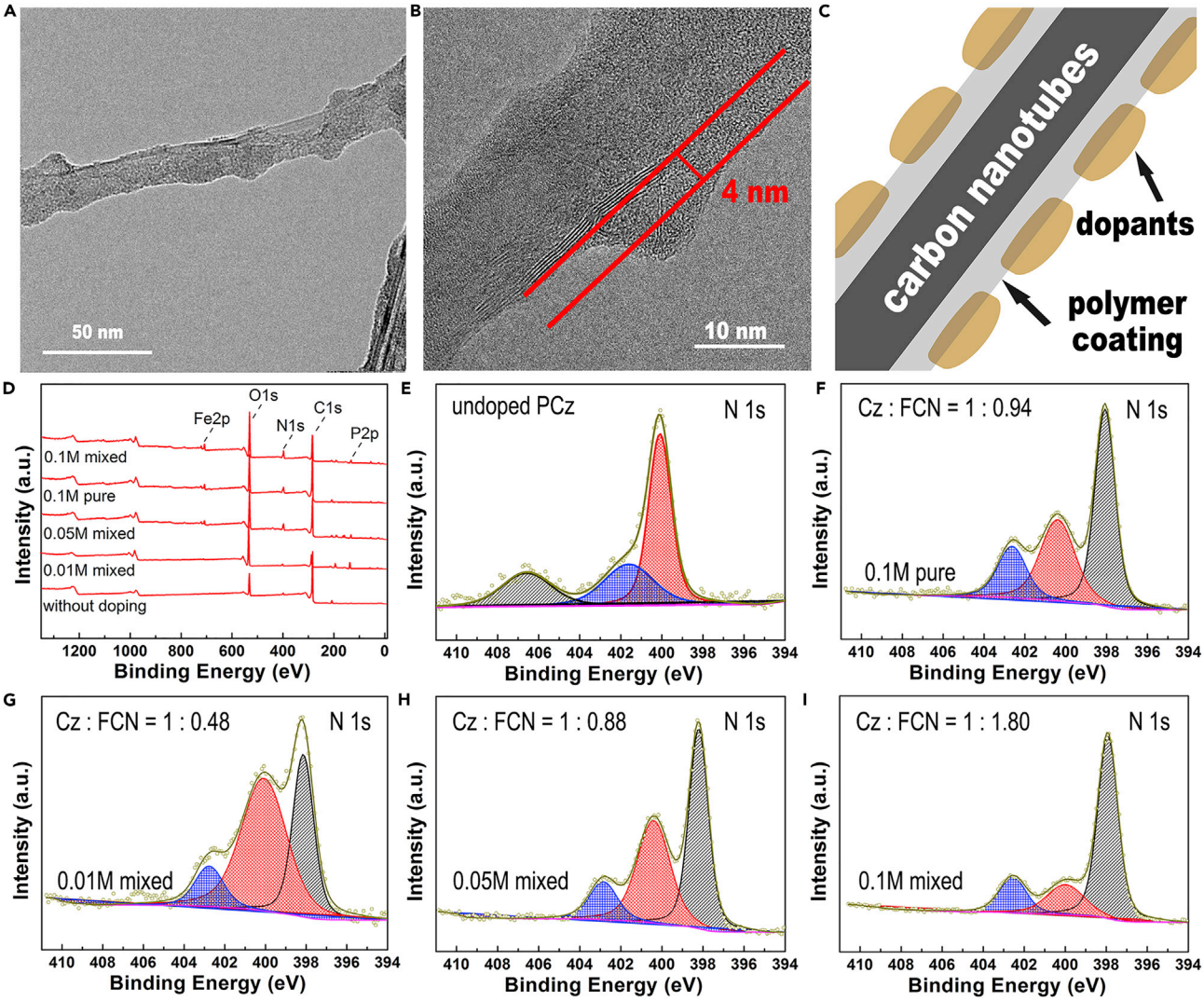

Figure 3. The Characterization and Quantitative Analysis of Composites

(A–C) (A and B) TEM images and (C) corresponding schematic diagram of the surface composition of the CNT/PCz:FCN composite.

(D–I) (D) Survey XPS spectra and (E–I) N 1s XPS spectra of the doped/undoped CNT/PCz composites.

The lowest and highest ratios of 1:0.48 and 1:1.80 were obtained for the PCz doped by 0.01 and 0.1 M mixed solutions, and similar ratios of 1:0.88 and 1:0.94 were obtained for that doped by 0.05 M mixed solutions and 0.1 M pure FCN solutions. Thus, we can draw a conclusion that doping levels of PCz can be effectively controlled by the types and concentrations of dopants via the first polymerization and second doping processes. Moreover, the CNT/PCz:FCN composite with the stabilization of PO is promising to apply in the Li-O_2 cells owing to the high surface area, quick electron transfers, and abundant redox sites on the composite surface.

The Controllable and Preferable Electrochemical Performance of CNT/PCz Composites

The redox properties of CNT/PCz:FCN composites are consistent with the above-mentioned results of PCz:FCN composites (Figures 4A and 4B), accompanying with a significant n-type behavior and an increase in doping levels. Meanwhile, CNT/PCz composites doped by mixed solutions have lower redox potentials without any peak separation existing in that doped by pure FCN solutions. Although an apparent increase of current densities was discovered at the same scan rate in Figure 4A, a polarization phenomenon of potentials happened between oxidation and reduction peaks, which was probably caused by enhanced contents of dopants in the CNT/PCz composite.

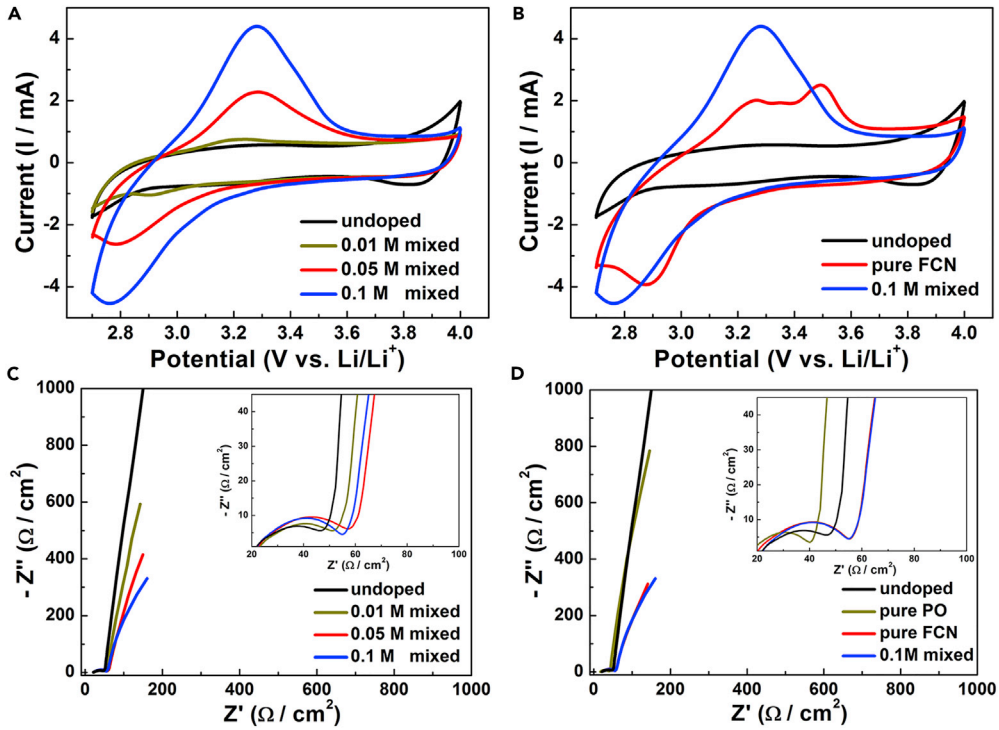

Figure 4. The Redox Properties and Conductivity of Different Composites

(A and B) Voltammograms of PCz films undoped and doped by (A) mixed solutions with different concentrations as well as (B) the pure solutions for comparision on the substrate of CNT films from 2.7 V to 4.0 V vs Li/Li^+ at 20 mV s^{-1}.

(C and D) Complex plane impedance plots around open circuit potentials of the CNT/PCz composites undoped and doped by (C) mixed solutions with different concentrations as well as (D) the pure solutions for comparision.

The charge transfer process and electronic conductivity of CNT/PCz:FCN composites are definitely crucial for their applications to energy storage systems. Therefore, EIS measurements were conducted at the composite/electrolyte interface. The equivalent circuit model we chose includes two resistances in parallel with respective constant phase elements (CPEs), which has been reported for the composite electrodes of carbon materials and polymers as illustrated in Figure S8A (Ates, 2011; Chen et al., 2003). As for CNT films covered by organic semiconductor coatings, the electrical circuit of Rsc//CPE is proposed in series with that of Rct//CPE, where Rct is the resistance of charge transfer at the contact interface of composites and Rsc is the resistance of space charge layer for redox processes (Zhu et al., 2012). The impedance data were definitely fitted to the electrical circuit Rs-(Rct//CPE_1)-(Rsc//CPE_2) by means of complex nonlinear least squares (CNLS, Figures S8B and S9). The complex plane impedance plots are shown in Figures 4C and 4D, and results from the CNLS fitting are listed in Table S1. In the high-frequency part, the curved region of impedance plots is related to the charge transfer process, and a slight increase of Rct (varying from 32.40 Ω/cm^2 to 41.84 kΩ/cm^2) in Figure 4C implies that a higher doping density can influence the charge transfer at the interface, which may lead to the above-mentioned polarization of potentials in CV curves. However, the decrease of impedance data over the low-medium frequencies is pretty evident and the values of Rsc range from 44.92 to 1.66 kΩ/cm^2 via deeply doping processes, illustrating that the conductivity of PCz can be effectively improved. This result is consistent with the improvement of carrier concentrations and related to the variation of the distance between V_{FB} and orbital energy levels. To determinate the respective effect of two dopants on the electrochemical process, we carried out EIS tests on CNT/PCz composites doped by pure solutions (Figure 4D). The PO ions can reduce the Rct in semicircle regions of impedance plots to facilitate the charge transfer compared with undoped samples. Although FCN ions increase the Rct, it can greatly decrease the Rsc over the low-medium frequencies for redox processes of organic polymer layers, proving that it works as a crucial dopant to improve the conductivity of PCz. Considering the prior effect of FCN ions on the redox properties and conductivity of CNT/PCz composites, the little impact of FCN on the charge transfer process at the composite interface can be avoided since the whole electrochemical performance is preferable for the catalytic process in Li-O_2 cells.

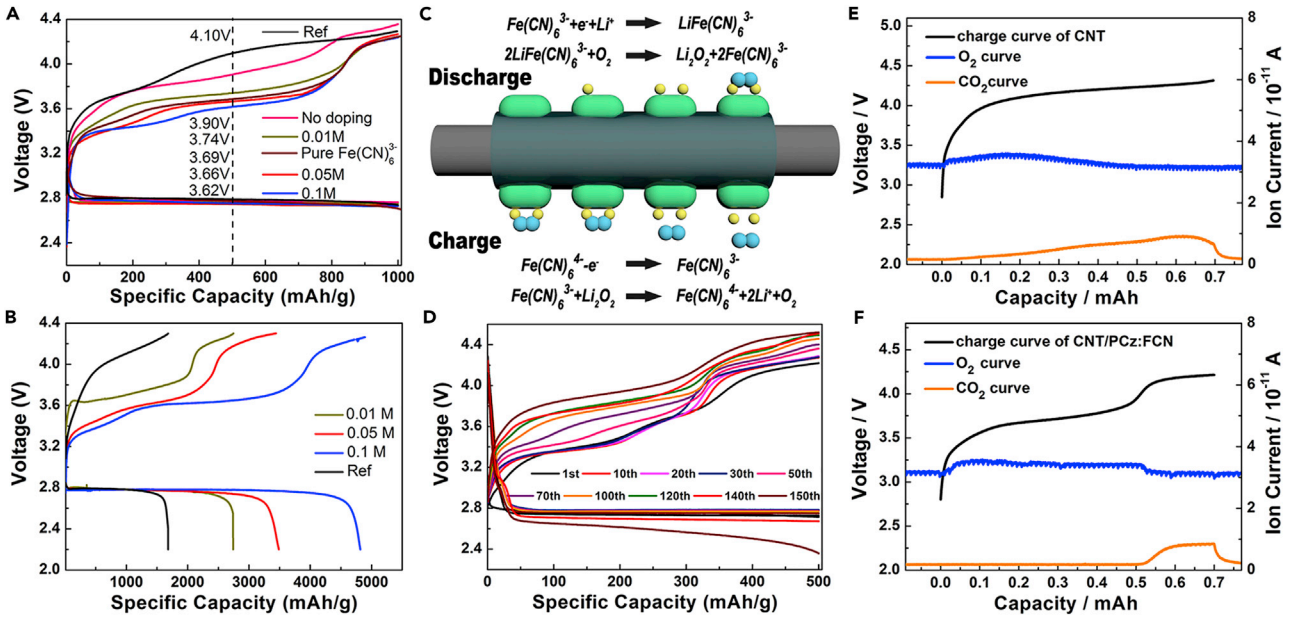

Figure 5. The Charge-Discharge Data and DEMS Analysis of Composite Electrodes in Li-O_2 Cells

(A) First cycle of Li-O_2 cells using different CNT/PCz:FCN composite electrodes at a current density of 0.1 mA cm^{-2} for the limited capacity of 1,000 mAh g_{CNT}^{-1}.

(B) Full cycle of Li-O_2 cells at 0.1 mA cm^{-2}.

(C) Schematic diagram of bifunctional catalysis of FCN dopants on the charge-discharge process.

(D) Cycle performance of Li-O_2 cells using the CNT/PCz composite electrode doped by a 0.1 M mixed solution for 500 mAh g_{CNT}^{-1}.

(E and F) *In situ* DEMS measurements of Li-O_2 cells using (E) the pristine CNT electrode and (F) the CNT/PCz:FCN composite electrode during the charge process.

The Bifunctional Catalysis and the Protective Effect of PCz:FCN Coatings in Li-O_2 Cells

The CNT film covered by n-type organic coatings is adopted as a free-standing electrode in Li-O_2 cells to improve the electrochemical performance and cyclability. The galvanostatic charge-discharge profiles in Figure 5A were obtained in the electrolyte of 1 M $LiClO_4$/DMSO with a limited capacity of 1,000 mAh/g_{CNT} at a current density of 0.1 mA/cm^{-2} (about 200 mA/g_{CNT}), where the CNT film occupies at least two-thirds of the amount of electrodes. The reduced overpotentials and enhanced energy efficiencies are definitely achieved by further doping processes, and the biggest drop of charge voltages is 0.48 V compared with that of the pristine CNT film. The carbon electrode covered by organic coatings has been reported in Li-O_2 cells to lead to a somewhat lower discharge capacity due to the decrease of active surface areas (Kim and Park, 2017). On the contrary in our work (Figure 5B), discharge capacities of surface-doped samples can be regularly enhanced with the values ranging from 1,800 to 4,800 mAh/g_{CNT}, which may be attributed to abundant electro-active sites and increased doping levels of PCz:FCN coatings. The SEM images of discharge products are shown in Figure S10. Small disc-shaped Li_2O_2 particles were accumulated in the gaps among the CNT fibers for the pristine CNT electrode. With the coating of doped polymers, the morphology of Li_2O_2 tends to be big and toroidal, which is beneficial to the formation of products and improvement of discharge capacities (Liu et al., 2017).

The schematic diagram of the bifunctional catalysis of CNT/PCz:FCN composites during charge-discharge processes is illustrated in Figure 5C. When $Fe(CN)_6^{3-}$ ions are first electro-reduced during discharging, they can combine with lithium ions (Li^+) and then provide reactive sites for reduced oxygen species to facilitate the formation of main products Li_2O_2. However, as illustrated in Figure S11, $Fe(CN)_6^{3-}$ ions cannot always catalyze the reduction of oxygen since discharge voltages are discovered to be slightly improved at the beginning of discharge. This result implies that, when the products Li_2O_2 cover the surface of composite electrode, $Fe(CN)_6^{3-}$ ions cannot combine with the Li^+ ions and oxygen. Simultaneously in the charge process, the $Fe(CN)_6^{4-}$ ions are first electro-oxidized on the surface of electrodes; then it catalyzes the decomposition of Li_2O_2, generating O_2 by chemical oxidation. The charge transfer at the composite/electrolyte interface and the conductivity of PCz is very critical to ensure the bifunctionality of redox

dopants during electrochemical processes, which has been proven to be feasible through the verification of CV and EIS results.

Another important property of organic coatings was pointed out by some researchers that this protective layer can enhance cycling life by the suppression of side reactions between the carbon electrode/organic electrolyte and carbon electrode/Li_2O_2 interfaces (Amanchukwu et al., 2016; Kim and Park, 2017), which is a serious challenge for carbon materials to apply to Li-O_2 cells. In addition, surface-doped PCz synthesized in our work has been proven to be beneficial to the electrochemical stability at higher voltages. Thus, an excellent cycling performance was obtained with the electrode of the CNT/PCz composite doped by a 0.1 M mixed solution, maintaining a constant capacity and the most of charge voltages under 4.0 V over 150 cycles (Figure 5D). The charge overvoltages definitely increased after cycles, which is a common result for the solid catalysts in Li-O_2 cells (Lin et al., 2018) and may be caused by the accumulation of side products.

The verification of the protective effect of PCz:FCN coatings was realized via *in situ* differential electrochemical mass spectrometry (DEMS) tests, which were performed on the charging of pristine CNT films and CNT/PCz:FCN composites. As illustrated in Figures 5E and 5F, when charging the cells with different electrodes to the original discharge capacity in Ar, variation trends of the gas evolutions of O_2 and CO_2 are clearly different from each other. During the charging process for the pristine CNT electrode (Figure 5E), the gas evolutions of O_2 and CO_2 appeared simultaneously at the beginning of the voltage rise, which indicates the existence of parasitic reactions that are caused probably by the instability of carbon materials. In comparison, during a gentle voltage rise around a low platform for the CNT/PCz:FCN electrode (Figure 5F), only the evolution of O_2 was detected owing to the catalysis of PCz:FCN composites. Then a sudden voltage rise at the end of charging accompanied the evolution of CO_2. This is an inevitable voltage polarization that can lead to the decomposition of electrolytes, which also appears in other solid catalysts and can be effectively solved by the incorporation of soluble catalysts. Although we did not carry out the quantitative study of ratios of electrons per gas molecule, this qualitative result of DEMS can strongly support the effect of a PCz:FCN coating on the enhanced cycling performance in Li-O_2 cells.

DISCUSSION

In fact, the introduction of functionalized dopants in the CPs matrixes during the polymerization has been investigated as an effective strategy to obtain a bulk-doped polymer with high conductivity and stability (Pron and Rannou, 2002). Nevertheless, in electrocatalysis and energy storage systems, the insufficient utilization of redox dopants and the attenuation of electrochemical responses are inevitable challenges for bulk-doped polymers since the selectivity and doping levels of different dopants are hard to control during the polymerization.

In this work, we demonstrated the feasibility of a controllable electro-doping strategy after the polymerization with FCN dopants as redox-active centers and PO dopants as structural stabilizers, where the doping levels and semiconductor properties of surface-doped PCz are effectively adjusted to obtain a preferable electrochemical performance. A stable cation inserting/expulsing behavior of this composite is verified by EQCM measurements. When using the CNT films as the free-standing substrate, the CNT/PCz:FCN composite is definitely suitable to work a highly active catalytic electrode in Li-O_2 cells. The molecule-level dispersed FCN dopants on the surface and the whole conductivity supported by the CNT fibers make sure this composite owns the bifunctional catalysis and provides abundant redox sites to facilitate the formation and decomposition of products Li_2O_2. Simultaneously, the organic protective coatings can obviously suppress the side reactions of carbon materials and expand their application in the electrocatalysis under the oxidation environment.

Limitations of Study

We believe this organic-inorganic hybrid design can become a promising strategy not only for Li-O_2 cells but also for other electrocatalysis and energy storage systems since it can effectively improve the conductivity, redox activity, and electrochemical stability of CPs and provide more flexible selectivity of organic materials. Nevertheless, the nanostructures of polymers and the ratios of multiple dopants could be further optimized for the better electrochemical performance. Moreover, the catalytic mechanism of this composite in electrochemical systems could be further investigated with more *in situ* methods.

METHODS

All methods can be found in the accompanying Transparent Methods supplemental file.

SUPPLEMENTAL INFORMATION

Supplemental Information can be found online at https://doi.org/10.1016/j.isci.2019.03.016.

ACKNOWLEDGMENTS

This work was supported by the National Natural Science Foundation of China (No. U1802256, 51672128, 21773118, 51802154), the Key Research and Development Program in Jiangsu (BE2018122), Priority Academic Program Development of Jiangsu Higher Education Institutions (PAPD).

AUTHOR CONTRIBUTIONS

C.X. designed the experiments, conducted most of the characterizations, and wrote the manuscript. L.W., S.H., and H.X. helped to synthesize the materials and collected the data. X.Z. designed the systems, analyzed the data, and commented on the manuscript.

DECLARATION OF INTERESTS

The authors declare no competing interests.

Received: November 21, 2018
Revised: January 30, 2019
Accepted: March 14, 2019
Published: April 26, 2019

REFERENCES

Amanchukwu, C.V., Gauthier, M., Batcho, T.P., Symister, C., Shao-Horn, Y., D'Arcy, J.M., and Hammond, P.T. (2016). Evaluation and stability of PEDOT polymer electrodes for Li-O_2 batteries. J. Phys. Chem. Lett. *7*, 3770–3775.

Arrondo, J.L.R., Goñi, F.M., and Macarulla, J.M. (1984). Infrared spectroscopy of phosphatidylcholines in aqueous suspension a study of the phosphate group vibrations. Biochim. Biophys. Acta *794*, 165–168.

Ates, M. (2011). Review study of electrochemical impedance spectroscopy and equivalent electrical circuits of conducting polymers on carbon surfaces. Prog. Org. Coat *71*, 1–10.

Aurbach, D., McCloskey, B.D., Nazar, L.F., and Bruce, P.G. (2016). Advances in understanding mechanisms underpinning lithium-air batteries. Nat. Energy *1*, 16128.

Baba, A., Tian, S., Stefani, F., Xia, C., Wang, Z., Advincula, R.C., Johannsmann, D., and Knoll, W. (2004). Electropolymerization and doping/dedoping properties of polyaniline thin films as studied by electrochemical-surface plasmon spectroscopy and by the quartz crystal microbalance. J. Electroanal. Chem. *562*, 95–103.

Boudreault, P.-L.T., Wakim, S., Blouin, N., Simard, M., Tessier, C., Tao, Y., and Leclerc, M. (2007). Synthesis, characterization, and application of indolo[3,2-b]carbazole semiconductors. J. Am. Chem. Soc. *129*, 9125–9136.

Burn, P.L., Grice, A.W., Tajbakhsh, A., Bradley, D.D.C., and Thomas, A.C. (1997). Insoluble poly [2-(2'-ethylhexyloxy)-5-methoxy-1,4-phenylenevinylene] for use in multilayer light-emitting diodes. Adv. Mater. *9*, 1171–1174.

Chen, W.C., Wen, T.C., and Teng, H.S. (2003). Polyaniline-deposited porous carbon electrode for supercapacitor. Electrochim. Acta *48*, 641–649.

Christensen, J., Albertus, P., Sanchez-Carrera, R.S., Lohmann, T., Kozinsky, B., Liedtke, R., Ahmed, J., and Kojic, A. (2012). A critical review of Li/air batteries. J. Electrochem. Soc. *159*, R1–R30.

Ehsani, A., Bigdeloo, M., Ansari, M.Y., Mirtamizdoust, B., Heidari, A.A., Hadi, M., and Shiri, H.M. (2018). Nanocomposite of conjugated polymer/nano-flowers Cu(II) metal-organic system with 2-methylpyridinecarboxaldehyde isonicotinohydrazide as a novel and hybrid electrode material for highly capacitive pseudocapacitors. Bull. Chem. Soc. Jpn. *91*, 617–622.

Hamadou, L., Aïnouche, L., Kadri, A., Yahia, S.A.A., and Benbrahim, N. (2013). Electrochemical impedance spectroscopy study of thermally grown oxides exhibiting constant phase element behaviour. Electrochim. Acta *113*, 99–108.

Hillman, A.R. (2011). The EQCM: electrogravimetry with a light touch. J. Solid State Electrochem. *15*, 1647–1660.

Karon, K., and Lapkowski, M. (2015). Carbazole electrochemistry: a short review. J. Solid State Electrochem. *19*, 2601–2610.

Kim, J., Kim, J.H., and Ariga, K. (2017). Redox-active polymers for energy storage nanoarchitectonics. Joule *1*, 739–768.

Kim, J.Y., and Park, Y.J. (2017). Carbon nanotube/Co_3O_4 nanocomposites selectively coated by polyaniline for high performance air electrodes. Sci. Rep. *7*, 8610.

Kim, S.Y., and Song, H.-K. (2015). Conducting polymers with functional dopants and their applications in energy, environmental technology, and nanotechnology. Clean. Technol. *21*, 12–21.

Klavetter, F.L., and Grubbs, R.H. (1988). Polycyclooctatetraene (polyacetylene): synthesis and properties. J. Am. Chem. Soc. *110*, 7807–7813.

Liang, Y., Chen, Z., Jing, Y., Rong, Y., Facchetti, A., and Yao, Y. (2015). Heavily n-dopable pi-conjugated redox polymers with ultrafast energy storage capability. J. Am. Chem. Soc. *137*, 4956–4959.

Lin, X., Yuan, R., Cai, S., Jiang, Y., Lei, J., Liu, S.-G., Wu, Q.-H., Liao, H.-G., Zheng, M., and Dong, Q. (2018). An open-structured matrix as oxygen cathode with high catalytic activity and large Li_2O_2 accommodations for lithium–oxygen batteries. Adv. Energy Mater. *8*, 1800089.

Liu, C., Brant, W.R., Younesi, R., Dong, Y., Edström, K., Gustafsson, T., and Zhu, J. (2017). Towards an understanding of Li_2O_2 evolution in Li–O_2 batteries: an in operando synchrotron X-ray diffraction study. ChemSusChem *10*, 1592–1599.

Lu, J., Li, L., Park, J.B., Sun, Y.K., Wu, F., and Amine, K. (2014). Aprotic and aqueous Li-O_2 batteries. Chem. Rev. *114*, 5611–5640.

MacDiarmid, A.G. (2001). "Synthetic metals": a novel role for organic polymers. Angew. Chem. Int. Ed. *40*, 2581–2590.

McCloskey, B.D., Scheffler, R., Speidel, A., Girishkumar, G., and Luntz, A.C. (2012a). On the mechanism of nonaqueous Li-O_2 electrochemistry on C and its kinetic overpotentials: some implications for Li-air batteries. J. Phys. Chem. C *116*, 23897–23905.

McCloskey, B.D., Speidel, A., Scheffler, R., Miller, D.C., Viswanathan, V., Hummelshoj, J.S., Norskov, J.K., and Luntz, A.C. (2012b). Twin problems of interfacial carbonate formation in nonaqueous Li-O_2 batteries. J. Phys. Chem. Lett. *3*, 997–1001.

Milczarek, G., and Inganas, O. (2012). Renewable cathode materials from biopolymer/conjugated polymer interpenetrating networks. Science *335*, 1468–1471.

Mozaffari, S., Nateghi, M.R., Behjat, A., and Borhani-Zarandi, M. (2012). Effects of dopants and copolymerization on Schottky barriers of polypyrrole and polyindole/metal interfaces. Iran. Polym. J. *21*, 799–808.

Ottakam, M.M., Freunberger, S.A., Peng, Z., and Bruce, P.G. (2013). The carbon electrode in nonaqueous Li-O_2 cells. J. Am. Chem. Soc. *135*, 494–500.

Pandey, P.C., and Panday, D. (2016). Novel synthesis of nickel–iron hexacyanoferrate nanoparticles and its application in electrochemical sensing. J. Electroanal. Chem. *763*, 63–70.

Pron, A., and Rannou, P. (2002). Processible conjugated polymers: from organic semiconductor to organic metals and superconductors. Prog. Polym. Sci. *27*, 135–190.

Qi, Z., and Pickup, P.G. (1998). Restructuring of cationic conducting polymers by $Fe(CN)_6^{4-}$. J. Electroanal. Chem. *441*, 131–137.

Rajesh, Pandey, S.S., Kumar, D., Takashima, W., and Kaneto, K. (2004). Electrochemomechanical deformation studies of $[Fe(CN)_6]^{3-}$ ion doped conducting polypyrrole film. Thin Solid Films *467*, 227–230.

Shi, Y., Peng, L., Ding, Y., Zhao, Y., and Yu, G. (2015). Nanostructured conductive polymers for advanced energy storage. Chem. Soc. Rev. *44*, 6684–6696.

Song, H.-K., and Palmore, G.T.R. (2006). Redox-active polypyrrole: toward polymer-based batteries. Adv. Mater. *18*, 1764–1768.

Song, Z., Qian, Y., Liu, X., Zhang, T., Zhu, Y., Yu, H., Otani, M., and Zhou, H. (2014). A quinone-based oligomeric lithium salt for superior Li–organic batteries. Energy Environ. Sci. *7*, 4077–4086.

Tóth, P.S., Endrődi, B., Janáky, C., and Visy, C. (2015). Development of polymer–dopant interactions during electropolymerization, a key factor in determining the redox behaviour of conducting polymers. J. Solid State Electrochem. *19*, 2891–2896.

Xia, J., Masaki, N., Lira-Cantu, M., Kim, Y., Jiang, K., and Yanagida, S. (2008). Effect of doping anions' structures on poly(3,4-ethylenedioxythiophene) as hole conductors in solid-state dye-sensitized solar cells. J. Phys. Chem. C *112*, 11569–11574.

Xu, J.J., Xu, D., Wang, Z.L., Wang, H.G., Zhang, L.L., and Zhang, X.B. (2013). Synthesis of perovskite-based porous $La_{0.75}Sr_{0.25}MnO_3$ nanotubes as a highly efficient electrocatalyst for rechargeable lithium-oxygen batteries. Angew. Chem. Int. Ed. *52*, 3887–3890.

Yu, J., Luo, J., Chen, Q., He, K., Meng, F., Deng, X., Wang, Y., Tan, H., Jiang, H., and Zhu, W. (2014). Synthesis and optoelectronic properties of a novel dinuclear cyclometalated platinum(II) complex containing triphenylamine-substituted indolo[3,2-b]carbazole derivative in the single-emissive-layer WPLEDs. Tetrahedron *70*, 1246–1251.

Zhan, J., Deng, S., Zhong, Y., Wang, Y., Wang, X., Yu, Y., Xia, X., and Tu, J. (2018). Exploring hydrogen molybdenum bronze for sodium ion storage: performance enhancement by vertical graphene core and conductive polymer shell. Nano Energy *44*, 265–271.

Zhou, M., Qian, J., Ai, X., and Yang, H. (2011). Redox-active $Fe(CN)_6^{4-}$-doped conducting polymers with greatly enhanced capacity as cathode materials for Li-ion batteries. Adv. Mater. *23*, 4913–4917.

Zhou, Q., and Shi, G. (2016). Conducting polymer-based catalysts. J. Am. Chem. Soc. *138*, 2868.

Zhu, X.M., Guo, Y., Xing, Z.Q., and Lei, M.K. (2012). Effect of nitrogen on semiconducting properties of passive films of a high nitrogen face-centered-cubic phase formed on austenitic stainless steel. J. Electrochem. Soc. *159*, C319–C325.

ISCI, Volume *14*

Supplemental Information

A Heavily Surface-Doped Polymer with the Bifunctional Catalytic Mechanism in Li-O_2 Batteries

Chengyang Xu, Langyuan Wu, Shifan Hu, Huamei Xie, and Xiaogang Zhang

Supplemental Information

A Heavily Surface-Doped Polymer with The Bifunctional Catalytic Mechanism in Li-O_2 Batteries.

Chengyang Xu, Langyuan Wu, Shifan Hu, Huamei Xie, and Xiaogang Zhang

Supplemental Figures

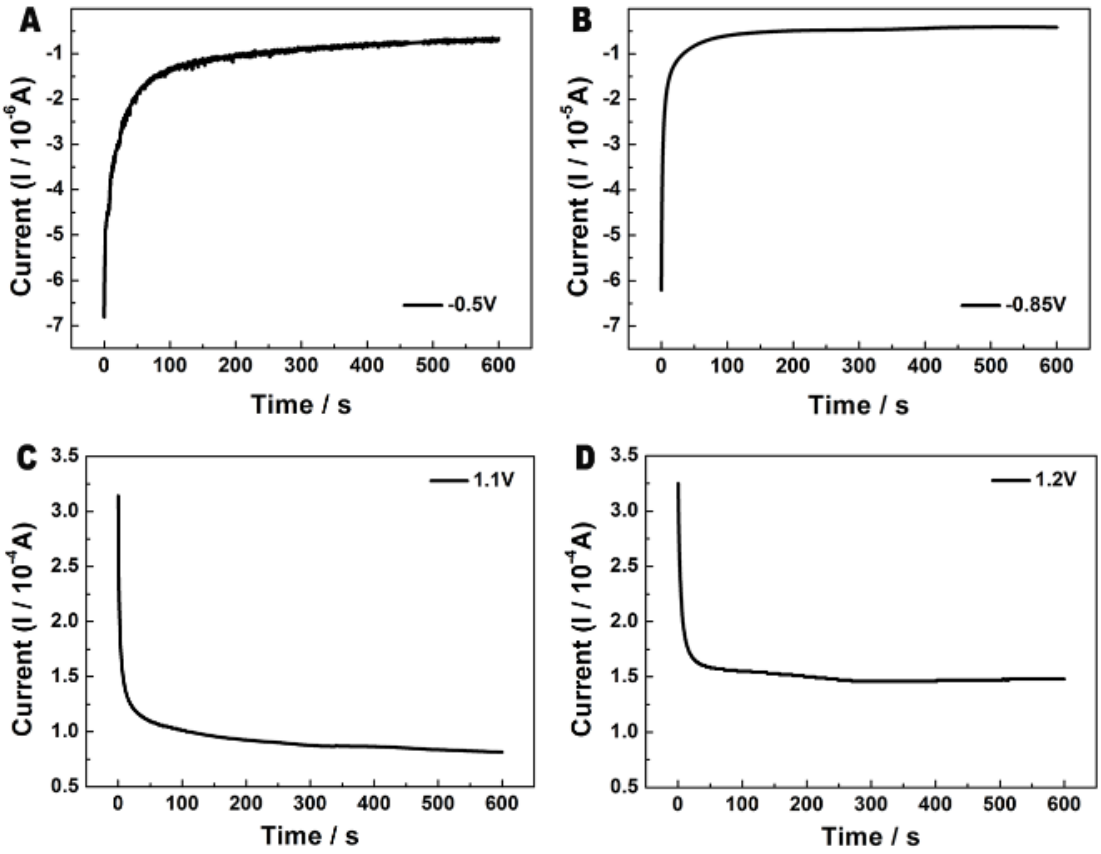

Figure S1, The first dedoping and second doping processes of as-synthesized PCz, related to Figure 1.

Two dedoping processes respectively for 10 min at constant potentials of (A) -0.5 V and (B) -0.85 V vs. Ag/Ag^+; two doping processes respectively for 10 min at constant voltages of (C) 1.1 V and (D) 1.2 V vs. Ag/Ag^+.

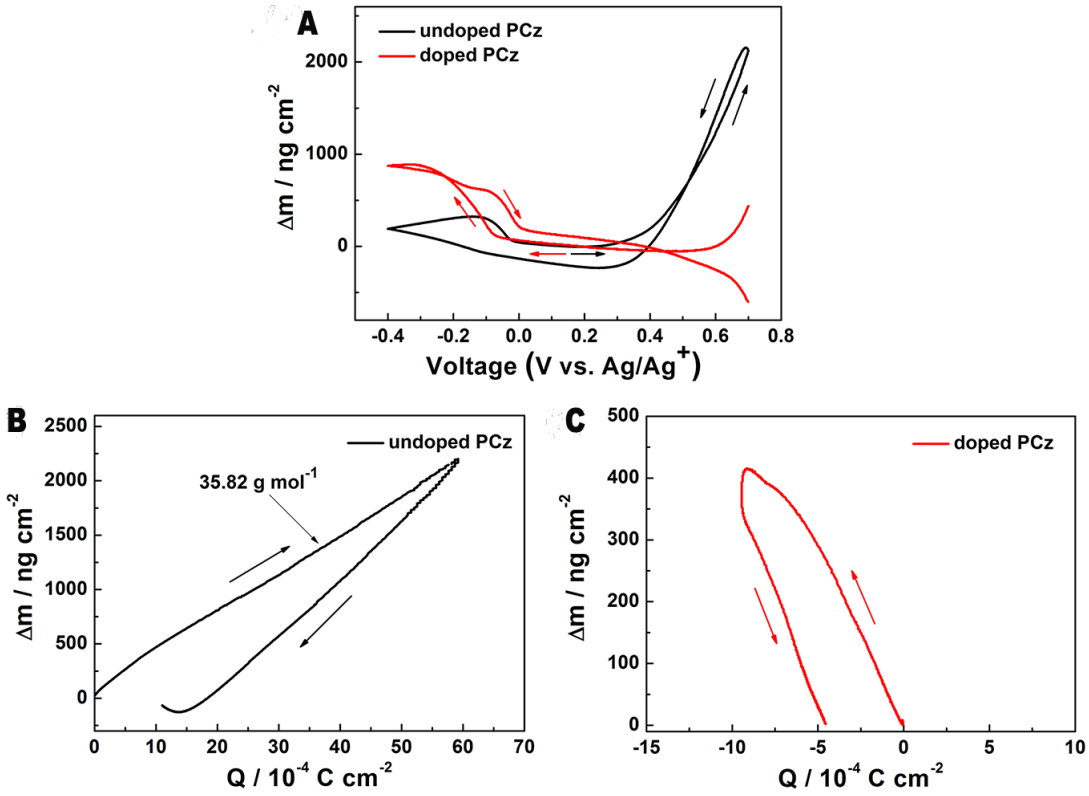

Figure S2, EQCM analysis, related to Figure 1.

(A) Gravimetric responses to a successful redox cycling in the solution of $LiClO_4$/ACN of undoped (black line) and doped (red line) PCz. Plots of mass change versus charge density in limited redox cycling of (B) undoped and (C) doped PCz.

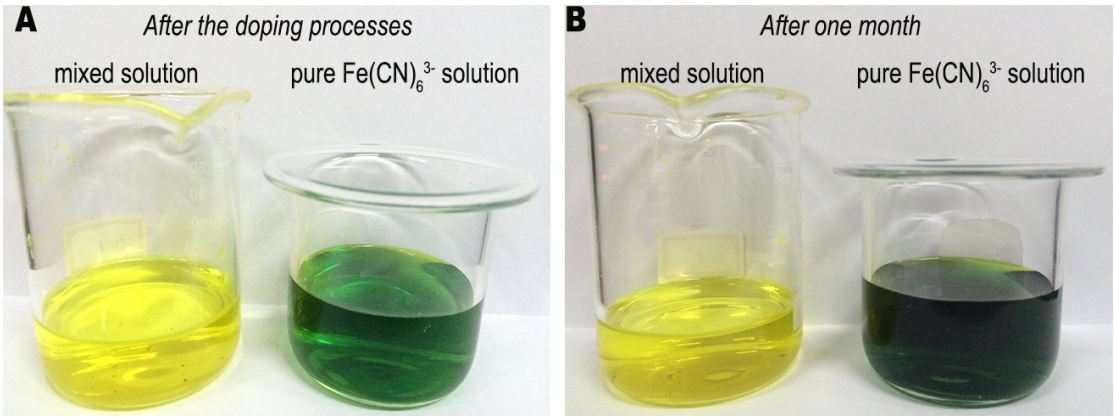

Figure S3, Digital photographs of doping solutions, related to Figure 2.

Digital photographs of mixed doping solutions and pure $Fe(CN)_6^{3-}$ solutions just after doping processes (A) and after being laid aside for one month (B).

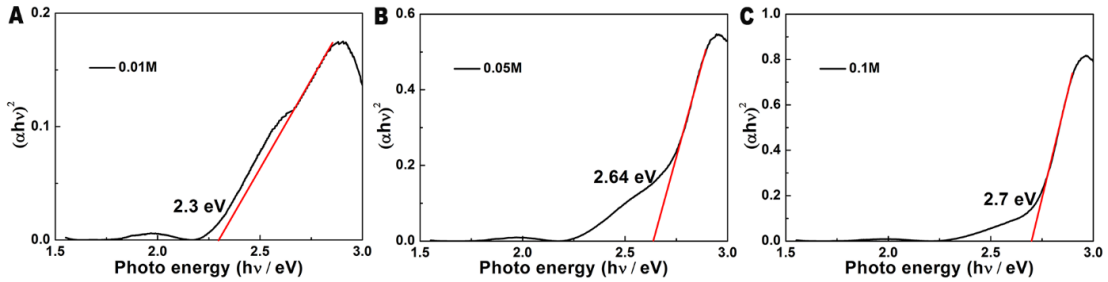

Figure S4, $(\alpha h\nu)^2$~hν plots, related to Figure 2.

$(\alpha h\nu)^2$~hν plots from UV-Vis spectrum showing the optical band gaps of PCz doped by (A) 0.01 M, (B) 0.05 M, and (C) 0.1 M mixed doping solutions.

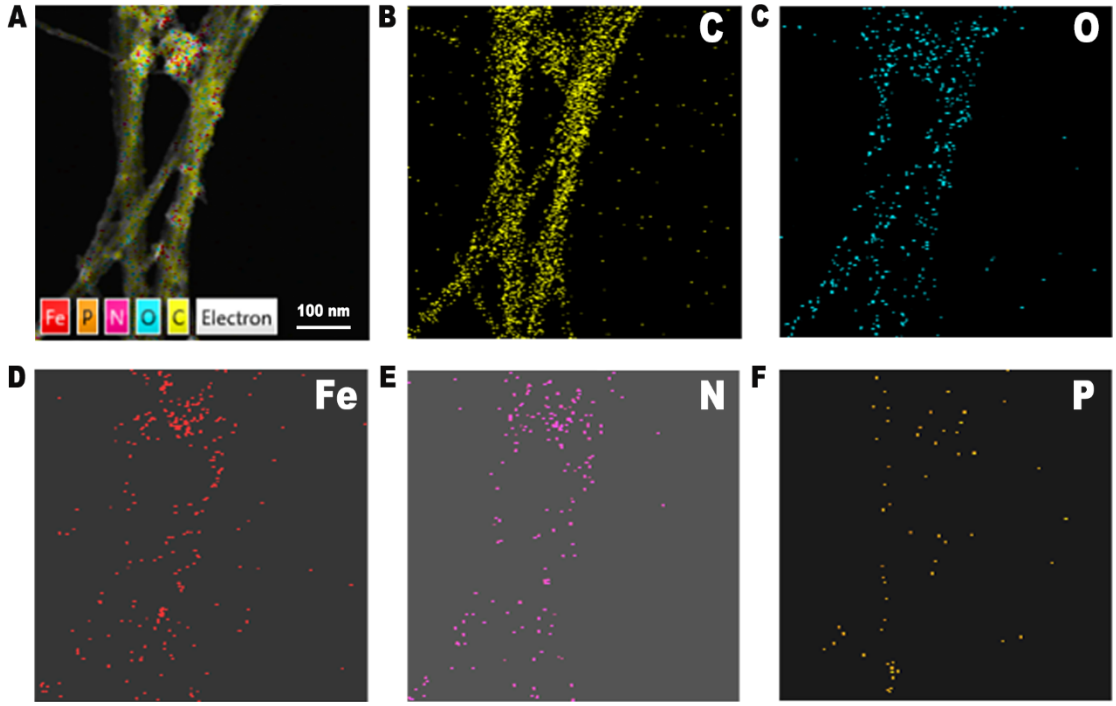

Figure S5, TEM and elemental mapping images, related to Figure 3.

TEM image (A) of PCz doped by 0.1 M mixed solution, corresponding elemental mapping images of carbon (B), oxygen (C), iron (D), nitrogen (E), and phosphorus (F).

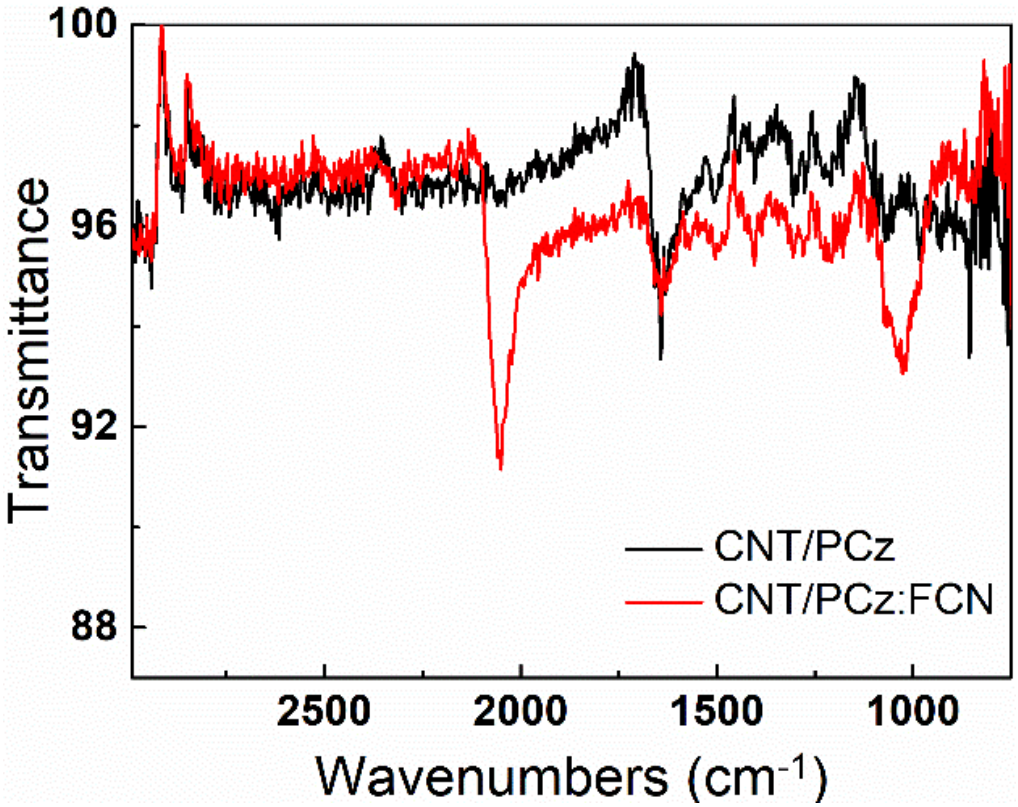

Figure S6, FTIR spectra, related to Figure 3.

FTIR spectra of the composites of CNT/PCz and CNT/PCz:FCN.

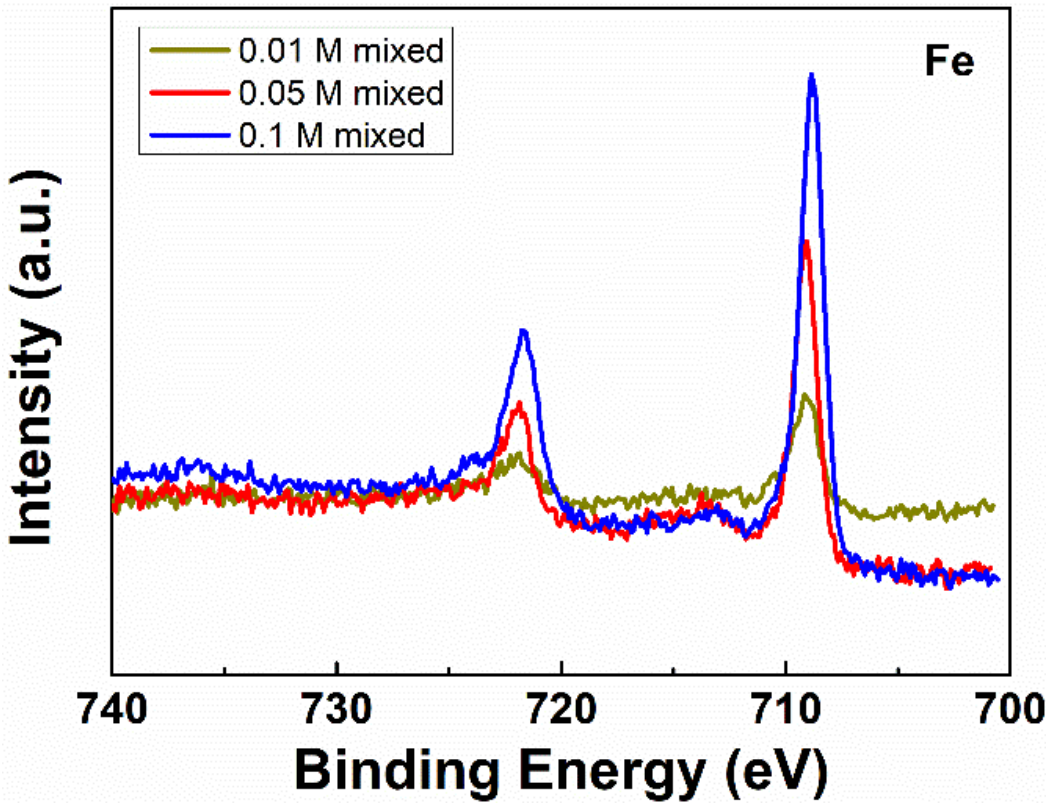

Figure S7, Fe2P XPS spectra, related to Figure 3.

Fe2P XPS spectra of CNT/PCz:FCN composites.

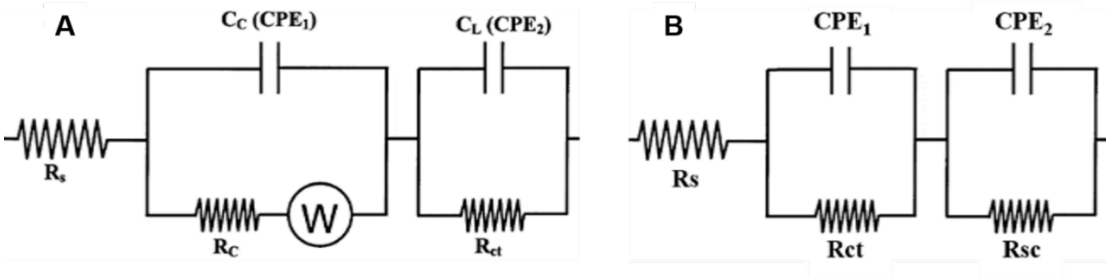

Figure S8, Equivalent circuits, related to Figure 4.

The equivalent circuits for composite electrodes of (A) reported result and (B) this study.

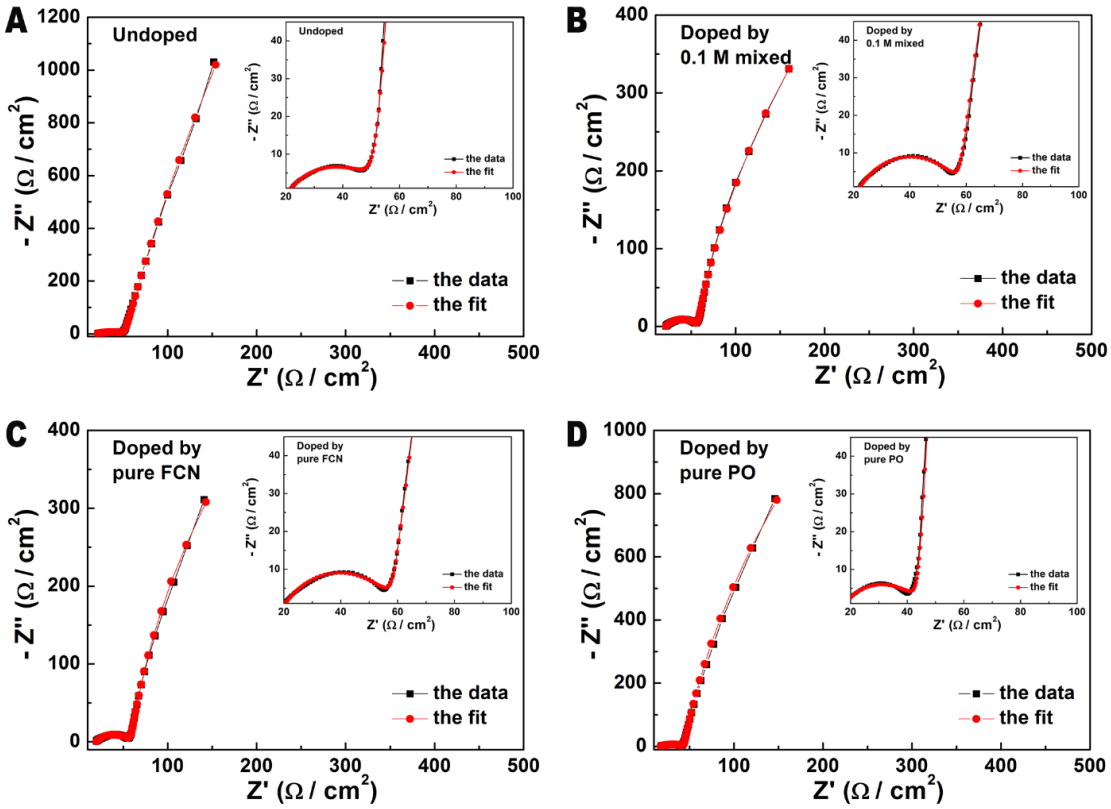

Figure S9, Complex plane impedance plots, related to Figure 4.

Complex plane impedance plots (black lines for the primary data and red lines for the fits) of undoped CNT/PCz composite (A) and these composites doped in solutions of 0.1 M mixed dopants (B), 0.1 M pure $Fe(CN)_6^{3-}$ (FCN) (C), and 0.1 M pure PO_4^{3-} (PO) (D), fitted to the equivalent circuit of Rs-(Rct//CPE_1)-(Rsc//CPE_2).

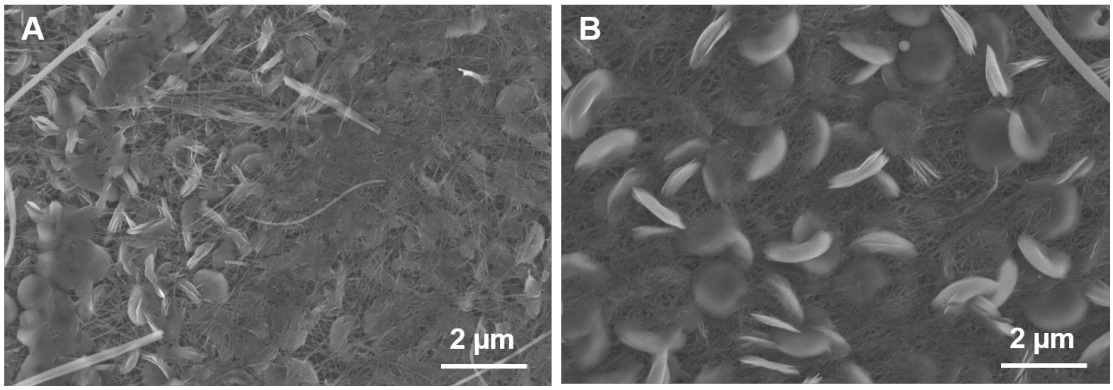

Figure S10, SEM images of discharge products, related to Figure 5.

SEM images of the different cathode after discharge with a limited capacity of 1000 mAh/g_{CNT}: (A) pristine CNT electrode, (B) composite electrode of CNT/PCz:FCN.

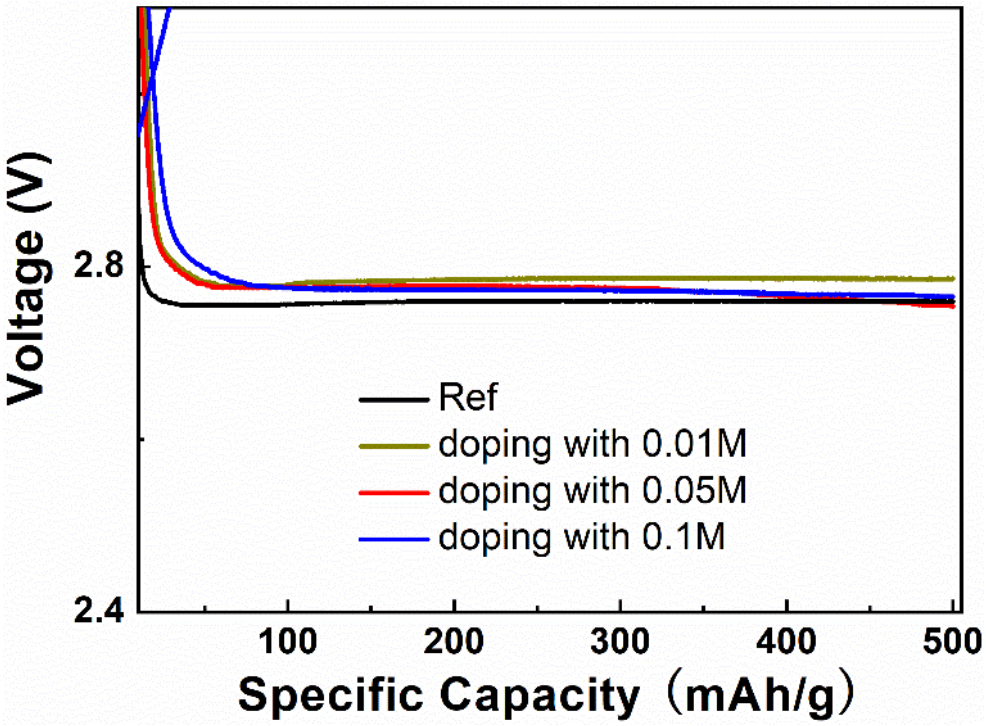

Figure S11, Discharge curves, related to Figure 5.

The enlarged view of discharge curves of composite electrodes as well as pristine CNT electrode (the black line named Ref).

Supplemental Table

Table S1, CNLS results derived from the equivalent circuit of Rs-(Rct//CPE_1)-(Rsc//CPE_2) around open circuit potentials, related to **Figure 4**.

Samples	Rs $\Omega\ cm^{-2}$	R_{ct} $\Omega\ cm^{-2}$	$\emptyset_1$	T_1 $10^6\Omega^{-1}s^{n1}cm^{-2}$	R_{sc} $k\Omega\ cm^{-2}$	$\emptyset_2$	T_2 $10^6\Omega^{-1}s^{n1}cm^{-2}$
Undoped	20.67	**32.40**	0.4846	1.324	**44.92**	0.9513	13.56
Doped by 0.01 M mixed	22.73	**30.16**	0.5569	0.741	**4.691**	0.9983	22.63
Doped by 0.05 M mixed	21.62	**41.84**	0.5249	0.941	**3.866**	0.9323	25.00
Doped by 0.1 M mixed	21.47	**37.04**	0.5699	0.609	**1.662**	0.9199	34.65
Doped by 0.1 M pure FCN	19.651	**39.51**	0.5453	0.7121	**2.230**	0.9216	39.04
Doped by 0.1 M pure PO	16.973	**27.54**	0.5215	0.8864	**11.54**	0.9591	17.95

Transparent Methods

Chemicals

Carbazole, ammonium phosphate tribasic ($(NH_4)_3PO_4$), potassium ferricyanide ($K_3Fe(CN)_6$) and acetonitrile (ACN) were purchased from Aladdin and were used as received. Lithium perchlorate ($LiClO_4$, Aladdin) was dried under vacuum. The solvent dimethyl sulphoxide (DMSO, Aladdin) was distilled with CaH_2 under vacuum, and dried over activated molecular sieves for a week. Ultra-light carbon nanotube film (CNT film, Jiedi, Suzhou, China) was acidized at 90 °C for 10 h in concentrated nitric acid, and punched into a disc with the loading area of 1.13 cm^2 and the weight of 0.4 mg.

The electrochemical processes of dedoping and doping

A common method to introduce large anions into the polymer matrixes is to add dopants into the same solution of monomers during the polymerization process. Our surface-doping method is achieved in two solutions after the polymerization for the different solubility of $Fe(CN)_6^{3-}$ and carbazole monomers. Firstly, the polycarbazole films are electro-dedoped in a 0.1 M $LiClO_4$/ACN solution at two constant potentials of -0.5 V and -0.85 V respectively for 10 min. Then, they are elctro-doped in a 0.1 M $(NH_4)_3PO_4/H_2O$ solution with different concentrations of $K_3Fe(CN)_6$ at two constant potentials of 1.1 V and 1.2 V respectively for 10 min. Since $Fe(CN)_6^{3-}$ ions are immobilized in the PCz matrixes and cannot dissolve in ACN or DMSO solutions, they are not released in organic solutions during subsequent electrochemical testing.

Electrochemical quartz crystal microbalance (EQCM) tests.

The EQCM tests were carried out in a special gas-flow enabled three-electrode cell (ALS Co., Ltd., Japan), in which the quartz crystal was used as the working electrode, coordinating with a platinum counter and a Ag/Ag^+ reference electrode. The quartz crystals were 8 MHz AT-cut gold electrodes (Chenhua Co., Shanghai, China) with a electrochemically active area of 0.196 cm^2. Crystal impedance measurements and cyclic voltammetry tests were performed using a CHI 440C EQCM device (CH Instruments, U.S.A). The mass change per unit area ($\Delta m/ng\ cm^{-2}$) is determined via the resonant frequency change ($\Delta f/Hz$) on the basis of the well-known Sauerbrey equation:

$$\Delta f = -\frac{2 f_0^2 \Delta m}{A(\rho_q \mu_q)^{1/2}} (\Delta m = -S\Delta f)$$

Where f_0 is the resonat frequency of the unload crystal, A is the electrochemically active area of Au electrode, ρ_q is the density of quartz and μ_q is the velocity of the acoustic wave in quartz. In this word, for a 8 MHz resonator, a proportionality factor S = 6.838 ng cm^{-2} Hz^{-1}.

The determination of the equivalent molar mass (M)

The equivalent molar mass of the anion and cation on the doping/dedoping processes were obtained based on the Faraday's law:

$$M = \frac{nmF}{Q}$$

Where $\Delta m/\Delta Q$ is the slope of a graph of Δm versus Q in Figure S2B, n is the number of electrons involved in the oxidation of one unit of PCz and faraday constant F = 9.65×10^4 C mol^{-1}. As for undoped PCz, the value of M for anions is 35.82 g mol^{-1} when we take n = 1.

Electrochemical Impedance Spectroscopy (EIS) measurements and Mott–Schottky (M-S) plots

EIS measurements were performed using a electrochemical workstation (ZIVE SP2, WonATech, Korea) in a three-electrode system with platinum counter electrode, Ag/Ag^+ reference electrode and the working electrode of glassy carbon and CNT film. To investigate the resistant of charge transfer, the EIS tests were performed around open circuit potentials and the frequency ranges from 0.01 Hz to 100 kHz with 5mV alternating signal. To obtain M-S plots, the direct current (dc) potential ranges from -0.4 V to 0.9 V in steps of 25 mV at a frequency of 10 kHz since the frequency dependence of the capacity-voltage curve is not affected. Prior to experiments, inert gas of argon was purged into the solution for ten minutes.

The determination of the band gaps (Eg)

The band gaps of PCz films doped by different solutions were estimated using the following formula according to the data of UV-Visible tests:

$$(\alpha h\nu)^2 = A(h\nu - Eg)$$

where α is the absorption coefficient, hν is the photon energy and A is a proportionality constant.

Assembly and electrochemical performance tests of Li-O_2 batteries

Battery assembly was carried out in an argon-filled glovebox with both oxygen and water contents less than 1 ppm. The coin cells consist of a lithium metal anode (12mm in diameter), a glass microfibre separator (Whatman D), a CNT/PCz:FCN composite cathode, and a stainless steel shell with holes in it. The galvanostatic discharge-charge

performance was conducted by the LAND–CT2001A battery-testing instrument (Wuhan Land Electronic Co. Ltd., China).

Differential electrochemical mass spectrometry (DEMS) experiments

DEMS experiments were carried out in a custom-built electrochemical flow cell (similar to EL-Cell, ECC-DEMS), which was attached in-line with a gas flow controller (MT-52, Horiba Metron) and a quadrupole mass spectrometer (HPR-1100, Inficon). The flow of Ar during the charge process was controlled at 1mL/min and prior to experiments, cells discharged to a setting capacity under oxygen atmosphere.

Characterization

The polycarbazole surface doped by redox-active dopants was observed using UV-visible spectroscopy (EL06043604, Varian Cary Eclipse) the transmission electron microscopy (TEM, FEI TECNAI-20), the X-ray photon spectroscopy (XPS, Perkin-Elmer PHI 550) with Al Kα as the X-ray source.